Acta Cryst A FOUNDATIONS ADVANCES
ISSN 2053-2733

Multipole electron densities and atomic displacement parameters in urea from accurate powder X-ray diffraction

Bjarke Svane,[a] Kasper Tolborg,[a] Lasse Rabøl Jørgensen,[a] Martin Roelsgaard,[a] Mads Ry Vogel Jørgensen[a,b] and Bo Brummerstedt Iversen[a]*

[a]Center for Materials Crystallography, Department of Chemistry and iNANO, Aarhus University, Aarhus, DK-8000, Denmark, and [b]MAX IV Laboratory, Lund, 22592, Sweden. *Correspondence e-mail: bo@chem.au.dk

Received 30 April 2019
Accepted 4 June 2019

Edited by A. Altomare, Institute of Crystallography - CNR, Bari, Italy

Keywords: electron density; powder diffraction; vacuum measurements; molecular crystals; synchrotron radiation.

Supporting information: this article has supporting information at journals.iucr.org/a

Electron density determination based on structure factors obtained through powder X-ray diffraction has so far been limited to high-symmetry inorganic solids. This limit is challenged by determining high-quality structure factors for crystalline urea using a bespoke vacuum diffractometer with imaging plates. This allows the collection of data of sufficient quality to model the electron density of a molecular system using the multipole method. The structure factors, refined parameters as well as chemical bonding features are compared with results from the high-quality synchrotron single-crystal study by Birkedal *et al.* [*Acta Cryst.* (2004), A**60**, 371–381] demonstrating that powder X-ray diffraction potentially provides a viable alternative for electron density determination in simple molecular crystals where high-quality single crystals are not available.

1. Introduction

Detailed knowledge of the nature of chemical bonding is a prerequisite for understanding the physical and chemical properties of materials, and experimentally this information is best available in the electron density (ED). Small deviations from spherical symmetry in the ED around each atom can be determined from accurate measurement of the intensity of X-ray Bragg reflections (Coppens, 1997). Virtually all experimental ED distributions have been determined from structure factors extracted from single-crystal X-ray diffraction (SCXRD) data, since this has been regarded as the optimal way to obtain data of the highest quality (Koritsanszky & Coppens, 2001; Jørgensen *et al.*, 2014). Accurate determination of the ED places much higher requirements on the quality of the measured data than conventional structure determination in terms of accuracy, high completeness and resolution. This is because of the increased number of parameters to be determined, but also because a change in ED will correlate with a change in the atomic displacement parameters (ADPs) (Bindzus *et al.*, 2014). For SCXRD, this means that several potential systematic errors must be accurately assessed before a reliable ED model can be obtained. The errors include absorption in the sample, and extinction effects in the low-angle intense reflections. Improper correction for these effects gives rise to systematic errors in the collected data, which reduce the quality of the obtained ED distributions as well as ADPs.

These systematic errors are essentially avoided in a powder X-ray diffraction (PXRD) measurement. The small crystallite size all but eliminates extinction effects, while absorption is

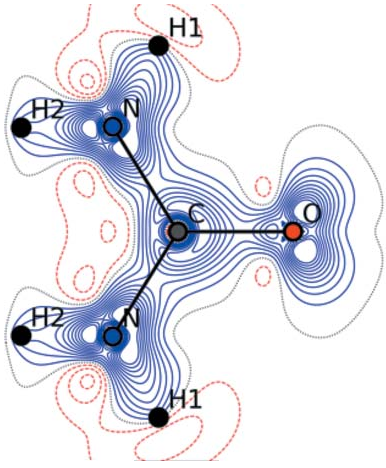

straightforward to treat due to powder sample homogeneity. Furthermore, all data are collected in a single exposure, removing the need to scale between frames. The advantages come at the cost of having to separate the intensity arising from overlapping peaks in the powder pattern and a more difficult background treatment. Correct assignment of intensity to neighbouring or even completely overlapping reflections is dependent on a good description of the peak shape and scattering model (Bindzus *et al.*, 2014). Background description is often carried out by fitting smoothly varying functions with a few parameters such as *e.g.* Chebyshev or Legendre polynomials. Imperfect modelling of the background will introduce systematic errors in the integrated intensity. Attaining PXRD data of sufficient quality for ED modelling critically depends on minimization of these disadvantages.

To that aim, we have developed the Aarhus vacuum imaging-plate diffractometer (AVID), which minimizes the background contribution by keeping the sample and primary beam in vacuum, thus essentially removing air scattering contributions to the background. The peak overlap is minimized through a large sample-to-detector distance of 1200 mm, reducing the relative instrumental broadening. The large radius also significantly improves the ratio of coherent to incoherent scattering, further minimizing the background signal. The reader is referred to the paper by Tolborg *et al.* (2017) for more information on the instrument.

Recent studies using AVID have shown remarkable results including modelling of subtle core electron deformation features for high-symmetry systems with small unit cells, where single-crystal (SC) measurements are severely affected by absorption and extinction effects (Wahlberg *et al.*, 2015, 2016; Bindzus *et al.*, 2014; Tolborg *et al.*, 2017). Here, we challenge determination of EDs from PXRD beyond two-atomic relatively simple structures to determine the current limits of the method. Molecular crystals without heavy elements have a relatively low absorption and only minor extinction effects. Additionally, the primary challenges of determining the ED based on PXRD data are increased as the symmetry in the system is decreased, and thus peak overlap becomes more significant. The main advantage of PXRD is that it places much lower requirements on crystal size and crystal quality. For systems that have a prohibitive size limitation or *e.g.* significant twinning issues, PXRD may be preferable. For some systems growing single crystals may even prove impossible, making PXRD the only method of obtaining X-ray structure factors. This does, however, require that a stable methodology for data collection and treatment is developed in the case of molecular crystals.

A further complication for molecular crystals lies in the deconvolution of ED deformation, atomic positions and ADPs, as these features correlate to a high extent (Bindzus *et al.*, 2014). This is a well-known problem especially for hydrogen atoms, where the bond lengths are often severely underestimated (Madsen *et al.*, 2004). The second part of this paper is thus to evaluate ADP determination based on PXRD data on molecular systems.

We have conducted a series of measurements on organic crystals at several wavelengths to determine the current limits of vacuum PXRD ED investigations and the best compromise between the signal-to-noise ratio of the Bragg intensities versus data resolution (both angular and scattering vector). The results presented here are on crystalline urea, which has been studied extensively using single-crystal diffraction methods (Swaminathan *et al.*, 1984; Spackman & Byrom, 1997; Zavodnik *et al.*, 1999; De Vries *et al.*, 2000; Spackman *et al.*, 1999; Birkedal *et al.*, 2004), providing ample results for comparison. In the charge density community, it is also well established as a benchmark system for development of new methods (Madsen *et al.*, 2013; Wall, 2016; Jayatilaka & Dittrich, 2008; Gatti *et al.*, 1994; Dovesi *et al.*, 1990). Here evaluation of the PXRD ED and ADPs for urea is primarily based on comparison with neutron diffraction data of Swaminathan *et al.* (1984), and high-quality single-crystal synchrotron X-ray data of Birkedal *et al.* (2004). The latter data are considered some of the most accurate data on organic molecular crystals in the literature. One could also choose to compare refined multipole model densities against theoretical calculations, and this has been done before (Nishibori *et al.*, 2007), but such comparison always carries the complication of whether thermal motion can be adequately deconvoluted from the experimental data. Our purpose is to assess the quality of the PXRD structure factors and corresponding refined parameters, and for this purpose the data of Birkedal *et al.* (2004) can be considered benchmark values.

Urea crystallizes in the tetragonal space group $P\bar{4}2_1m$, and has unit-cell dimensions a = 5.5780 (6), c = 4.6860 (7) Å

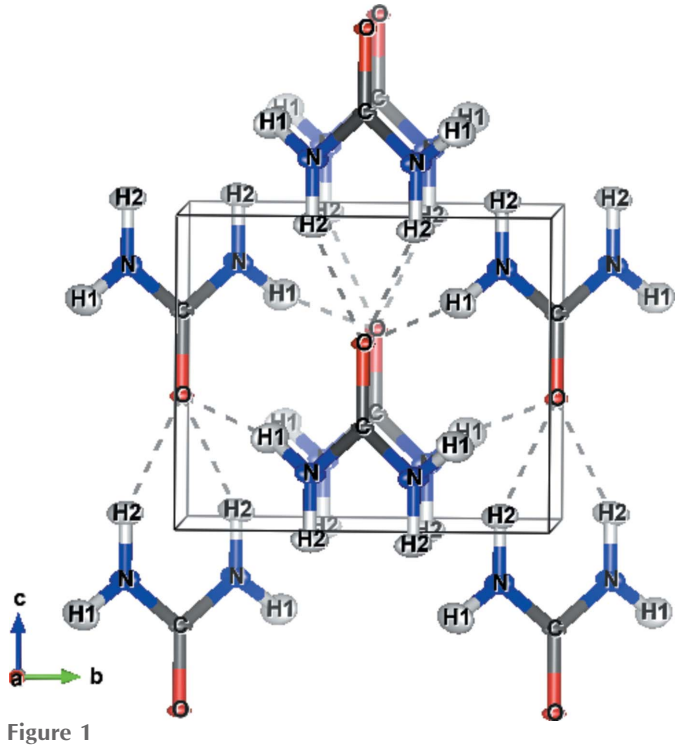

Figure 1
Urea crystal structure and atomic labelling scheme. The plot shows 50% probability ellipsoids based on harmonic anisotropic ADPs determined from PXRD measurements with λ = 0.49584 Å at 100 K.

(Birkedal *et al.*, 2004). This means that while there is significant overlap of peaks at high angles, there are still separated low-angle peaks to which the peak profile can be fitted. This makes it ideal as a first candidate for PXRD ED determination on non-centrosymmetric organic molecular crystals. The unit cell and atomic labelling scheme are shown in Fig. 1. Each molecule in the crystal is flat, with site symmetry *mm*2 for the C and O atoms, and *m* for the N and H atoms.

Urea crystals are known to have significant directional strain effects, particularly in the plane of the molecule (Birkedal *et al.*, 2004). This complicates the treatment of the peak profile, but all major whole-pattern (Rietveld) refinement programs have algorithms implemented to handle this (Weidenthaler, 2011). The more complex peak profile may, however, make proper separation of overlapping reflections more difficult.

2. Experimental details

2.1. Synchrotron powder X-ray diffraction measurement

Urea was purchased from Sigma–Aldrich as ACS reagent, 99.5%, CAS number 57-13-6. The large crystals were carefully ground, as any rough treatment resulted in severe strain-induced peak broadening. Annealing of the sample for 4 days at 363 K did not significantly reduce the broadening. After annealing, the sample was reground lightly, sieved (20 µm mesh) and packed in a 0.2 mm glass capillary. The capillary was rotated throughout the X-ray exposure.

PXRD data were collected using the AVID system at beamline P02.1 (Dippel *et al.*, 2015) and at beamline P08 (Seeck *et al.*, 2012), PETRA III. Both data sets were acquired at a sample temperature of 100 K. P02.1 operates at a fixed photon energy of ∼60 keV [λ = 0.20715 (5) Å], which in the AVID setup corresponds to a maximum measured resolution of $\sin(\theta)/\lambda$ = 2.41 Å^{-1}. The resolution was cut to $\sin(\theta)/\lambda$ = 1.26 Å^{-1} after the integration procedure, as significant peak intensities were not present at higher angles. The total exposure time was 300 min. The P08 data set was collected with a lower energy of 25.1 keV [λ= 0.49584 (2) Å] to reduce the peak overlap and increase the scattered intensity at the cost of reducing the $\sin(\theta)/\lambda$ resolution to 1.00 Å^{-1}. In these data, peaks were clearly present throughout the collected range. Furthermore, the incident flux was an order of magnitude higher, permitting faster experiments. The total exposure time for urea at P08 was 30 min. For both experiments, the beam size was cut to 0.3 × 0.3 mm using slits. Two-dimensional diffraction data were collected on four overlapping Fuji BAS-MS2040 image plates (IPs), which after exposure were digitized by a GE Typhoon FLA-7000 IP scanner.

To allow comparison with PXRD data obtainable from a modern synchrotron PXRD beamline, a data set was also collected at the powder diffraction beamline BL44B2 at SPring-8, Japan at 100 K (Kato *et al.*, 2010; Kato & Tanaka, 2016). A wavelength of λ = 0.50064 (5) Å was used with a maximum measured resolution of $\sin(\theta)/\lambda$ = 1.25 Å^{-1}. The detector at this beamline was also an IP, and both the specific IP and scanner were identical to the ones used in AVID.

2.2. Integration

After digitization, the data were corrected for IP decay as described by Straasø *et al.* (2013) and scanner position error as described by Tolborg *et al.* (2017). The scanner position correction is based on NIST standard Si (NIST 640d) and LaB_6 diffraction (NIST 660b) and has a resolution limited by the number of reflections in these materials. Earlier AVID studies have used a secondary scanner correction based on single peak fitting to the diffraction data to account for the lack of perfect determination of the scanner position, but the many overlapping peaks at high angles preclude this in the present case. The integration path is based on the intersection between the cylindrical AVID detector arc and the Debye–Scherrer cones. The IP position and rotation are determined based on difference minimization against a simulated diffraction pattern on the arc surface. This integration routine is explained in detail in Section S1 of the supporting information. Significant effort has been put into reducing the observed peak asymmetry, by *e.g.* fitting the IP roll angle and correcting for the deviation from a perfect cylinder of the arc. Uncertainties are based on sample statistics of each pixel contributing to the intensity in each 2θ bin in the diffractogram (Wahlberg *et al.*, 2016). Pixel size anisotropy has been determined independently and is applied in the integration process (Tolborg *et al.*, 2017).

3. Data quality on organic molecular crystals

Correct division of intensity between overlapping reflections critically depends on a good angular resolution to appropriately determine the peak profile. Initial experiments used short wavelengths to capture reflections to the highest possible resolution. Increased overlap and reduced scattering power mean that the data quality is inferior to that collected at longer wavelengths, as can be seen in Fig. 2. The data sets are scaled to have the same integrated intensity as the (110) reflection.

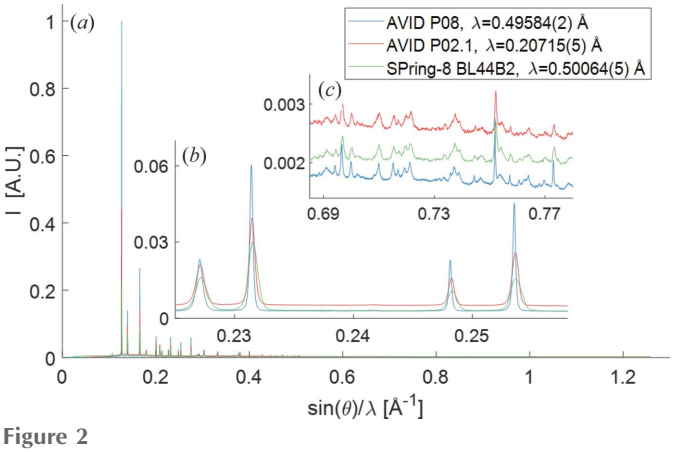

Figure 2
Integrated PXRD data collected at different wavelengths. The data sets are scaled to have the same integrated intensity as the (110) reflection.

Inspection of individual peaks [Fig. 2(*b*)] reveals that the peak width of long-wavelength AVID data (P08) is lower than for the other data sets, thus significantly reducing peak overlap. Comparison of the high-order data [Fig. 2(*c*)] shows that the peaks of the longer-wavelength data have a better signal-to-background ratio than the other data sets.

The difference between the AVID P08 data and the SPring-8 data shows the effect of performing diffraction in vacuum and having a large sample-to-detector distance, while the difference with respect to the P02.1 data is an effect of the increased Compton scattering relative to coherent scattering at higher X-ray energies. It is also of great importance, for the determination of the profile, that multiple points are present above the full width at half-maximum (FWHM) of the peaks. The wide peaks and high background of the SPring-8 data are problematic for accurate extraction of structure factors. They are included here for comparison with what can be obtained from a typical state-of-the-art synchrotron powder diffractometer.

The following sections primarily focus on the data collected at P08, PETRA III in April 2018, as these proved superior in terms of residuals, goodness of fit (GOF) and *R* factors after multipole modelling. Note that further modelling was attempted on all data.

4. Structure-factor extraction

Modelling of ED from PXRD follows a two-step process. First, structure factors are extracted using the Rietveld method. Second, the structure factors are modelled using the Hansen–Coppens multipole formalism to obtain the ED. 1D powder diffraction data were modelled using the Rietveld method in the program *JANA2006* (Petříček *et al.*, 2014). The methodology and refined parameters are described in Section S2. The observed structure factors were extracted using three different form-factor models: a conventional and simple independent atom model (IAM), a conventional Hansen–Coppens (HC) multipole model fitted to the reference single-crystal data (Birkedal *et al.*, 2004) and a more elaborate multipole model fitted to the same data. The conventional HC model included charge transfer between all atoms and all symmetry-allowed multipoles up to and including octupoles on C, O and N. For each H atom, all symmetry-allowed dipoles and quadrupoles were refined. No core deformation was included in the model (Fischer *et al.*, 2011). A radial expansion/contraction parameter (κ) was refined for all non-H atoms and set to 1.16 for H atoms based on a refinement against theoretical structure factors. The refinement used the Volkov–Macchi scattering bank based on relativistic density functional theory calculations (Volkov & Macchi, unpublished work). This model corresponds to the one used to model the extracted structure factors later. This model is termed MM. In the more complex model, multipolar functions to the hexadecapolar level are included for C, O and N. All κ are refined independently, and a single κ' was refined separately for each of the non-H atoms. In addition, anharmonic ADPs were refined for N and O atoms. This approximately corresponds to the model used in the single-crystal study of Birkedal *et al.* (2004) and this model is termed MM-HB. Using the ADP values from neutron diffraction (Swaminathan *et al.*, 1984) leads to much higher residuals. This is not surprising, as the neutron data were collected at 123 K whereas the PXRD data were collected at 100 K. Refining non-H-atom ADPs and scaling H-atom ADPs in the program *UijXN* (Blessing, 1995) was deemed the best option. Refined parameters are given in Section S2.

Table 1
Direct structure-factor comparison of temperature-corrected AVID extracted structure factors with reference SC data of Birkedal *et al.* (2004).

Residual factor $R(F) = \sum(|F - F_{ref}|)/\sum(F_{ref})$ and ratio average $\langle F/F_{ref}\rangle$.

	$R(F)$	$\langle F/F_{ref}\rangle$
IAM	0.0715	0.9976
MM	0.0775	1.0095
MM-HB	0.0767	1.0110

The aspherical form factors representing the static electron density of the individual pseudo-atoms could in principle come from other sources such as *e.g.* multipole fit to theoretical data, transferable atoms (Pichon-Pesme *et al.*, 1995; Volkov *et al.*, 2007) or Hirshfeld partitioning (Hirshfeld, 1977). The multipole model obtained from the SCXRD data was chosen here as it has previously been used as a reference in many studies of urea. Introducing a model for the aspherical form factors before extraction of structure factors will naturally bias the obtained values. If this was not the case, there would be no reason to introduce the model in the first place. This bias is small for low-order reflections without significant overlap but increases for higher-order reflections. It is expected that the severe peak overlap at high order will reduce the quality of extracted structure factors unless appropriate aspherical atomic scattering factors are used. Note that observed structure factors are extracted from the data, so the model is only used to divide intensities for overlapping reflections. The valence ED is primarily determined from the low-order reflections, where the overlap is limited.

Direct comparison of extracted structure factors for different extraction models with reference values allows evaluation of both the quality of the data, and of likely issues arising from the change in bias via atomic scattering factors. The agreement factors and the ratio averages are given in Table 1. The data are corrected for the temperature difference between measurements, which gives an angular dependence of the ratio. The corrected structure factors are given as $F_{obs,cor} = F_{obs} k \exp[B \sin^2(\theta)/\lambda^2]$, where k is a scaling constant and $B = 8\pi^2 \Delta U_{iso}$. Both k and B are determined based on a Wilson plot, *i.e.* a linear fit to the equation $\ln(F^2_{obs}/F^2_{ref}) = \ln(k) - 2B \sin^2(\theta)/\lambda^2$. The correction corresponds to a $\Delta U_{iso} =$ 0.0028–0.0030 Å^2 for all extraction models, which agrees very well with the expected difference in ADPs due to temperature differences when making a linear interpolation between 123 K and 60 K neutron data (Swaminathan *et al.*, 1984). A plot of the relative amplitude of extracted structure factors as a function of angle is given in Fig. 3.

Table 2
Refined parameters for multipolar models against different structure-factor lists.

AVID MM refers to PXRD data collected at λ = 0.49584 Å and structure factors extracted with MM refined on the SC reference data. AVID short λ refers to PXRD data collected at λ = 0.20715 Å and likewise extracted. AVID IAM-Ex was collected at λ = 0.49582 Å and structure factors were extracted with spherical atomic form factors. SC reference refers to structure factors from Birkedal *et al.* (2004) but refined with the MM model. Neutron refers to structure factors from Swaminathan *et al.* (1984) included for atomic position comparison. The population of individual multipolar functions is listed in the supporting information.

	AVID MM	AVID IAM-Ex	AVID short λ	SC reference	Neutron
R/*wR*	4.34/2.61	4.23/2.43	6.97/3.19	1.29/0.77	1.36/1.06
$(\sin\theta/\lambda)_{max}$ (Å^{-1})	1.00	1.00	1.26	1.44	0.77
No. of reflections ($I > 0$)	572	566	1184	1045	191
GOF	33.6	34.0	10.4	1.64	1.22
$\langle F_o/\sigma(F_o)\rangle$	2678	2738	487.6	367.8	865.2
z (C)	0.3287 (3)	0.3284 (4)	0.3280 (2)	0.32820 (4)	0.3284 (4)
z (O)	0.5955 (4)	0.5966 (5)	0.5966 (3)	0.59636 (4)	0.5971 (5)
x (N)	0.1445 (2)	0.1442 (2)	0.1448 (1)	0.14491 (3)	0.1448 (2)
z (N)	0.1773 (4)	0.1780 (4)	0.1782 (2)	0.17819 (4)	0.1786 (2)
P_V (C)	3.4 (2)	3.4 (2)	3.9 (2)	3.74 (4)	–
P_V (O)	7.1 (1)	7.0 (1)	6.81 (9)	6.51 (2)	–
P_V (N)	5.1 (2)	5.0 (2)	4.7 (1)	5.12 (3)	–
P_V (H1)	0.75 (8)	0.80 (8)	0.96 (5)	0.86 (1)	–
P_V (H2)	0.91 (7)	0.96 (7)	1.05 (5)	0.89 (1)	–
κ (C)	1.23 (4)	1.22 (4)	1.09 (2)	1.017 (4)	–
κ (O)	1.03 (1)	1.04 (1)	0.995 (8)	0.966 (2)	–
κ (N)	1.13 (3)	1.09 (3)	1.08 (2)	0.996 (3)	–

Direct structure-factor list comparison shows a reasonable agreement irrespective of extraction model. The degree of agreement is better for low-order data than for high-order data. The deviations of high-order reflections likely come from an improper background modelling. Because of the high number of peaks at high angles, overlap is severe, which complicates the accurate separation of background and peak contributions. The effect on valence ED distribution of a high uncertainty in high-order reflections is expected to be small. In contrast, the information on ADPs is primarily contained in the high-order data.

In general, it would be expected that aspherical atomic scattering factors would improve the quality of the extracted observed structure factors, especially for overlapping peaks, but based on the direct comparison, this does not appear to be the case. Overlap is primarily present at high angles, where the effect of aspherical atomic scattering factors is small. The observed behaviour therefore must be an effect of improper deconvolution of background and structural effects, which is especially challenging for reflections with large overlap. It has previously been shown that iterative extraction/modelling based on an initial IAM extraction is possible (Bindzus *et al.*, 2014). As the structure factors in the present case are good, even when extracted using spherical independent atoms, an iterative procedure was unnecessary.

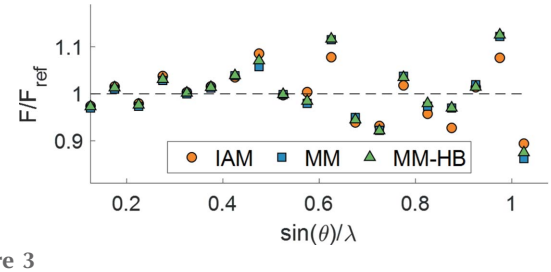

Figure 3
Binned relative structure-factor amplitude as a function of angle. No weighting has been applied to the reflections. The structure factors have been corrected for temperature difference as described in the text.

5. Hansen–Coppens multipolar modelling

As direct structure-factor comparison showed reasonable agreement irrespective of extraction model, an HC multipolar model was fitted to both IAM and MM extracted observed structure factors in *JANA2006*. The model included the same parameters as MM described earlier. Modelling of the SC reference structure factors was also done to the MM level to allow a direct comparison with PXRD data using identical models. The more extensive MM-HB model was also stable and gave physically sensible results on the reference SC data set, but not on AVID data and is thus not shown. Refined parameters are given in Table 2 and Fig. 4.

It is immediately clear that the AVID data sets qualitatively capture the same features as the SC reference. The atomic positions agree with the neutron positions within the uncertainty. The same overall charge transfer trends are also identified, but the magnitudes differ. The κ parameters refine to higher values for all AVID data sets than for the reference. On comparison with SC data, both the GOF and *R* factors show a worse agreement between data and model for the AVID data. The fractional coordinates agree fairly well (differences on the fourth digit), but the estimated uncertainty on AVID data is five to ten times larger than on SC data. This uncertainty is still underestimated, among others because of a finite point-spread function on the IPs, as is the uncertainty on the structure factors themselves, which does not include the uncertainty of the profile fit.

Between the AVID data sets, IAM extracted structure-factor lists are comparable in quality with those obtained from a more elaborate atomic scattering factor description. This is surprising and likely an effect of insufficient separation of

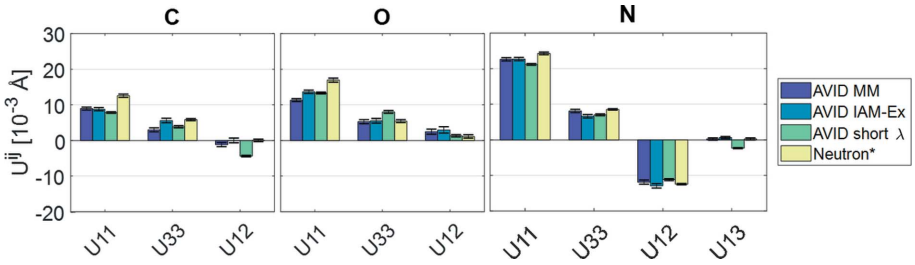

Figure 4
Refined ADPs from multipolar refinement on AVID data sets. Abbreviations for samples correspond to those in Table 2. Neutron* denotes approximate 100 K neutron ADPs based on linear interpolation between 60 K and 123 K and is included for reference. *U* values are given in tabular format in Table S2 in the supporting information.

background, thermal effects and ED distribution for the aspherical atomic scattering factor extraction. The long-wavelength data indeed do appear to give lower residuals than the short-wavelength data, indicating the advantage of more well-separated peaks and a lower background. Still, the increased noise in short-wavelength data is distributed around the same mean, as shown by the similar parameters.

In general, it is to be expected that the direction-independent terms reported in Table 2 are fairly stable with respect to extraction model compared with the directional multipolar terms. Agreement at this level is thus more an indicator of PXRD data quality than of reasonable intensity partitioning between overlapping reflections.

The ADPs obtained from multipole refinement indicate that the extraction model only slightly affects the ADP determination even for the polar bonds in urea. There are only minor differences between the MM and IAM extracted data sets. The limits of lower-quality data are also apparent, as AVID short λ deviates from the other two. Neutron data were collected at a higher temperature (123 K versus 100 K). To compare neutron values with those obtained from AVID, approximate neutron 100 K values are calculated based on linear interpolation between 60 K and 123 K data from Swaminathan *et al.* (1984). The signs and trends in ADPs are similar for all data sets, however, which points towards the AVID structure factors being reasonable. It is in itself satisfying to see that high-quality PXRD data can retrieve anisotropic ADPs in a molecular crystal. Although the quality of the PXRD data is not yet at the level of SCXRD, the same trends and approximately the same magnitudes are reached for all parameters.

To further investigate the quality of the ED models, deformation density and residual density maps are inspected. They are shown in Fig. 5 for the PXRD data extracted using IAM and MM and for the SC reference.

Overall, the trends described by all the data sets are the same. Charge is concentrated in all bonds, which corresponds well to the primarily covalent character of the bonds. The charge concentration around the O atom fits well with the expected lone pairs of oxygen with a double bond to carbon. There is qualitative agreement with both the reference and with results from the literature (Gatti *et al.*, 1994; Birkedal *et al.*, 2004). However, on closer examination, minor discrepancies can be seen. In particular, the negative lobes close to oxygen, which have elsewhere been used as an estimate of data quality (Morgenroth *et al.*, 2008), are not observed in the AVID data. While the N atom for both data sets has three lobes of charge concentration, the direction of these in the SC data is directly towards the neighbouring atoms. The models fitted to the AVID data [Figs. 5(*a*), 5(*b*)] show a twisted lobe that does not point straight towards the C atom. This affects the further analysis, as *e.g.* evaluation of properties in the bond critical point relies critically on the accurate determination of the position of this point. Similar problems are observed with oxygen lone pairs, albeit to a lesser degree. The charge accumulation around the nuclei is larger in the PXRD data due to the larger κ parameter. As the ADPs are lower than the scaled neutron values, both indicate that the model contracts more electron density around the average nuclei position. This may be an effect of too low background estimates at high angles. The difference in data quality is most clearly seen when comparing Figs. 5(*d*)–5(*f*). The residuals of the AVID data are much larger and show more prominent features around the atoms than the reference data. This is contrary to earlier AVID results on simpler systems with more perfect crystals such as *e.g.* Si (Tolborg *et al.*, 2017; Wahlberg *et al.*, 2016) or diamond (Bindzus *et al.*, 2014). In the present study of an organic molecular crystal the advantages of PXRD ED determination are reduced and the disadvantages increased. Despite the large difference in magnitude of residuals, residual density distribution analysis reveals that the errors are close to being

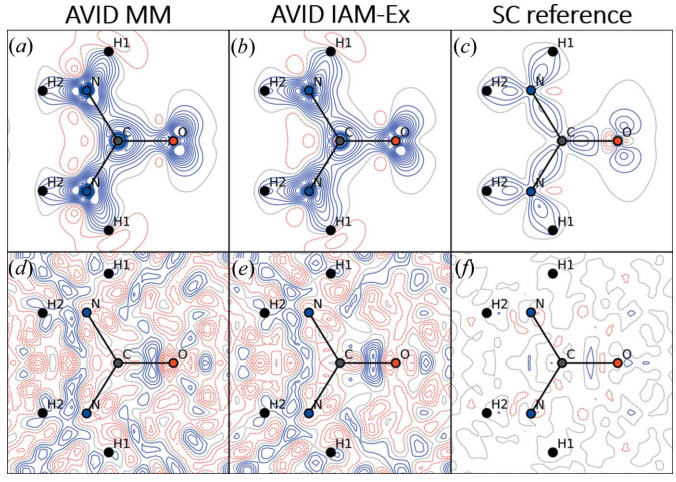

Figure 5
Real-space model evaluation of AVID MM (*a*), (*d*) and AVID IAM-Ex (*b*), (*e*) versus SC reference (*c*), (*f*). The [110] plane is shown centred on a single urea molecule. The plots show the static model deformation density (*a*)–(*c*) and residual density (*d*)–(*f*). Contour levels are 0.2 e Å^{-3} and 0.05 e Å^{-3}, respectively. Red contour lines are negative, blue are positive. Note that the SC reference is modelled using the MM model and not the full MM-HB model used in the original study by Birkedal *et al.* (2004). The residual density for this data set is improved by using the more extensive MM-HB model, where only random noise of low magnitude is observed.

normally distributed (see Figs. S3–S4 in the supporting information). The magnitude of residuals can then serve as a measure of the noise present in the data (Meindl & Henn, 2008).

To summarize, we have successfully determined the ED of a molecular crystal based on PXRD data. The quality of data was sufficient to allow structure-factor extraction without including a model for the aspherical atomic scattering factors – and indeed in this case it seems that the IAM extraction gives a structure-factor list of the same quality as the aspherical atomic scattering factor extraction. Deviations from the SC reference are observed and systematic trends in the residuals indicate incomplete modelling. The SC data are superior for the system studied here, but if SC data had been unavailable, the PXRD model gives a reasonable indication of the trends.

5.1. Deconvolution of atomic displacement from ED deformation

The challenge of deconvoluting ADPs from ED deformation is part of what initiated the study of vacuum PXRD as a method of obtaining the ED. A clear correlation between ED and ADP is observed even for light atoms such as carbon (Svendsen *et al.*, 2010). Deconvolution is complicated by the presence of systematic errors in SCXRD data, which affect data similarly to thermal motion. The systematic errors in PXRD data are much reduced as there are only negligible absorption and extinction effects, but it does come at the cost of requiring deconvolution of the background from the peak intensities.

Evaluation of the ADP determination is in this case challenged by the lack of a direct reference. The obvious choice would be neutron data, where the scattering is unaffected by the ED distribution, removing the deconvolution issue entirely. Though neutron data are available and have been used to estimate the H-atom positions and ADPs in the structure-factor extraction, they have been collected at a slightly different temperature. Here, we calculate the reference based on linear interpolation between ADPs from neutron diffraction data collected at 123 K and 60 K by Swaminathan *et al.* (1984) to estimate neutron ADPs at 100 K.

Usually, a good agreement between neutron and X-ray diffraction data is taken as an indicator of true ADPs in both cases (Iversen *et al.*, 1996; Morgenroth *et al.*, 2008; Fugel *et al.*, 2018). It should be noted that although neutron data are unaffected by the distribution of electrons, systematic errors still exist in the data. Disagreement between X-ray and neutron data is, therefore, not necessarily because the X-ray data are of low quality.

Comparison of ADPs between neutron, SCXRD and PXRD data for non-H atoms is given in Table 3. PXRD data using both short and long wavelengths and different extraction models are included. The data obtained from AVID were not of sufficient quality to successfully refine anisotropic hydrogen ADPs using the present methodology. Evaluation is based on the mean trace ratio, $\langle U^{ii}_{X}/U^{ii}_{N}\rangle$, the mean absolute difference of all U parameters, $\langle|\Delta U^{ij}_{X-N}|\rangle$, and the mean absolute difference of only the diagonal elements, $\langle|\Delta U^{ii}_{X-N}|\rangle$, of X-ray and neutron ADPs. Additionally, the root-mean-squared differences of X-ray and neutron ADPs weighted by the combined standard uncertainties, wRMSD = $\{\langle(U^{ij}_{X}-U^{ij}_{N})^2/[\sigma(U^{ij}_{X})^2+\sigma(U^{ij}_{N})^2]\rangle\}^{1/2}$, are calculated to also account for the systematic and random errors present in neutron data. This measure has previously been used to compare ADPs for both multipolar modelling and Hirshfeld atom refinement (HAR) with neutron data (Capelli *et al.*, 2014; Fugel *et al.*, 2018).

Table 3
ADP evaluation for PXRD and SCXRD.

Naming convention as in Table 2. Neutron reference based on linear interpolation between neutron 123 K and 60 K data sets by Swaminathan *et al.* (1984). SC reference by Birkedal *et al.* (2004) is compared with unscaled neutron values.

	$\langle U^{ii}_{X}/U^{ii}_{N}\rangle$	$\langle\lvert\Delta U^{ij}_{X-N}\rvert\rangle$	$\langle\lvert\Delta U^{ii}_{X-N}\rvert\rangle$	wRMSD
AVID short λ	0.87 (5)	0.0026 (6)	0.0029 (7)	6.42
AVID MM	0.79 (7)	0.0017 (9)	0.0024 (9)	3.67
AVID IAM-Ex	0.86 (7)	0.0014 (9)	0.0018 (9)	2.80
SC reference	1.03 (4)	0.0004 (4)	0.0003 (4)	1.59

The comparison in Table 3 shows that the ADPs determined from PXRD are further from reference neutron values than the reference SC data. However, even disregarding the potential discrepancy introduced from linear interpolation between neutron parameters at two different temperatures, the data presented here show that fairly accurate anisotropic ADPs can in fact be obtained from a PXRD measurement. The difference in ADP agreement between different extraction models indicates that the assignment of intensity of overlapping peaks is a primary limitation to the quality of the technique. This is supported by the fact that the short-wavelength data, which cover a large $\sin(\theta)/\lambda$ range but have increased peak overlap, are worse than the longer-wavelength data, where the multipolar model was more satisfactory and the peaks are more easily separated. It is surprising that IAM extracted structure factors agree more with neutron values than structure factors extracted using better atomic scattering factors. We do not expect this to be the general case, but rather an effect of the background and peak description in this particular data set.

5.2. Chemical bonding analysis

Chemical bonding is evaluated through the quantum theory of atoms in molecules (QTAIM) framework of determining properties in critical points (Bader, 2002). Bonds in particular can be described and classified using the properties of the ED in the bond critical points (BCPs). A critical point search was carried out on the ED model fitted to both MM and IAM extracted structure factors in *JANA2006*. Position and properties evaluated in the resulting BCPs are given in Table 4. The values are compared with the literature SC model of Birkedal *et al.* (2004) to evaluate the quality of a PXRD-derived ED model.

The bonds in urea have the typical characteristics of covalent (shared shell) interactions (Gatti, 2005). This is also found using the PXRD-based ED. The ED in the BCP is quite large while the Laplacian is negative, indicating a large degree of charge concentration. The PXRD data do not quantitatively recover the magnitude of this concentration in $\nabla^2\rho_{BCP}$, but this difference in values is not uncommon even in SCXRD studies (Zavodnik *et al.*, 1999). The determination of the total bond length shows good agreement between PXRD and SCXRD, whereas the BCP location on the bond path shows a significantly larger deviation. This also serves to explain the difference in $\nabla^2\rho_{BCP}$, as the Laplacian changes rapidly in the vicinity of the critical points.

The bond ellipticity, which gives an indication of the π and σ character of the bonds, also shows the same trends for PXRD data as for SCXRD data. An ellipticity around 0 would be expected for a σ-type bond. Birkedal *et al.* (2004) found that the ellipticity, bond length and charge density in the critical point indicated a charge delocalization between the O, C and N atoms and significant π character in the C—N bond. The refined ED distribution from PXRD indicates that this partial π character also includes the H2 atom, which from a chemical perspective is highly doubtful. The ellipticity is the ratio between two second-derivative values of the density, and thus it is highly dependent on minute details of the refinement.

The difference between extraction methods is quite distinct. The IAM extracted structure-factor list gives substantially better agreement with SC data. It was expected that aspherical atomic scattering factors would improve the ED determination, but in this case the opposite is observed. This serves to highlight the challenges involved in adequately separating peak intensities. The background description apparently absorbs the errors of the poor atomic scattering factors in the model based on IAM extracted structure factors.

The topological analysis of the PXRD-based ED shows that very satisfactory bond lengths and reasonable BCP properties can be determined. The PXRD data quality is sufficient to adequately capture the main ED features, while not being on a par with exceptional SCXRD data.

Table 4
BCP positions and properties in urea.

The first line is determined from AVID MM data, the second line is AVID IAM-Ex data. The third line is reference SC data (Birkedal *et al.*, 2004). R_x is the distance to the first atom listed. ε is the bond ellipticity.

	ρ_{BCP} (e Å^{-3})	$\nabla^2\rho_{BCP}$ (e Å^{-5})	R (Å)	R_x (Å)	ε
C—O	3.07	−13.4	1.2504	0.560	0.01
	2.82	−10.4	1.2565	0.540	0.01
	2.72	−31.8	1.2565	0.451	0.029
C—N	2.40	−2.0	1.3449	0.578	0.26
	2.36	−3.4	1.3422	0.574	0.25
	2.36	−25.0	1.3384	0.542	0.26
N—H1	2.40	−82.3	1.0097	0.843	0.12
	2.34	−58.4	1.0102	0.802	0.07
	2.25	−30.9	1.005	0.752	0.091
N—H2	2.24	−31.9	0.9949	0.769	0.13
	2.17	−24.0	0.9978	0.757	0.15
	2.28	−34.6	1.0020	0.749	0.073

6. Conclusion

We have successfully carried out multipole modelling of the ED of a molecular crystal based on PXRD data. Comparison with literature results reveals that the present PXRD data are noisier than high-quality SCXRD data. The refined multipole model parameters are significantly different between the PXRD and SCXRD data, but qualitatively the main chemical features of the ED are reproduced, as seen *e.g.* when comparing deformation density maps. This suggests that PXRD can offer a valuable alternative if conventional SCXRD measurements are problematic because of *e.g.* difficulty in obtaining adequately sized crystals or significant twinning issues.

Significant effort has been spent in reducing, adequately estimating and propagating errors in data reduction. This has primarily been done through optimization of the setup and the integration procedure. The uncertainties are estimated based on sample statistics along the integration path, which itself is based on a less idealized geometry than previously assumed, as shown in the supporting information. Evaluation of the errors after ED modelling shows that, while the errors are large in magnitude, they correspond well to random noise based on fractal dimension analysis (supporting information).

The primary limitation of the current setup is the quality of the detector system. Partitioning of intensity of overlapping reflections requires accuracy in the 2θ determination of each pixel. The current setup does not provide this. The position errors lead to erroneous estimates of the background, as the peak profile is widened to account for the small problems with peak position, accompanied by increased errors in partitioning of overlapping reflections. This in turn means accurate structure factors are most difficult to obtain at high angles, where overlap is severe. Wide, overlapping peaks with slightly wrong positions result in significant deviations in the ADPs. Attempting to reduce this issue via structure-factor extraction using aspherical atomic scattering factors was in this case not successful. This means that the primary issue is proper separation of the background from the peak intensity. The difficulty in intensity partitioning for highly overlapping peaks also places an upper limit on the unit-cell size of investigated systems, which is more restrictive than for SCXRD measurements. The method is also limited in application on systems with significant preferential orientation, which will correlate strongly with both ED and thermal parameters. Furthermore, the present PXRD data are challenged by significant strain effects.

The results of the ADP evaluation and topological analysis confirm that deconvolution of ED deformation and ADPs is difficult. It is therefore advisable to determine one of these parameters using a different method and then fix it in the refinement of the other parameter. This could *e.g.* be done by calculation of the theoretical aspherical atomic scattering factors prior to refinement of the ADPs. This is the basis of the HAR method (Capelli *et al.*, 2014; Woińska *et al.*, 2014, 2016; Fugel *et al.*, 2018).

The AVID project has focused on reducing the background contribution from air scattering and narrowing the diffraction peaks to reduce overlap. However, the main limitation in data quality is the detector technology. New photon-counting detectors are currently being implemented at many powder diffraction beamlines. In particular, MYTHEN detectors (Bergamaschi *et al.*, 2010) with impressive angular coverages, very low point-spread function and a large dynamic range may provide the necessary improvements in data quality. The main disadvantages in a common setup are the increased background contributions from both air and increased relative Compton scattering at short sample-to-detector distances, but this may prove less important than avoiding the detector issues that currently limit the quality of AVID data. Furthermore, a vacuum chamber and a large sample-to-detector distance can also be implemented for this type of detector.

7. Related literature

References cited in the supporting information: Alexander & Klug (1950), Le Bail *et al.* (1988) and Stephens (1999).

Acknowledgements

We gratefully acknowledge beam time at beamlines P02.1 and P08 at the PETRA III synchrotron, Deutsches Elektronen-Synchrotron DESY, Hamburg, a member of the Helmholtz Association (HGF), and the great support provided by the beamline teams and infrastructure group. We thank Hilmar Burmester for lending us critical equipment at very short notice. We also acknowledge Henning B. Pedersen from JJ X-ray A/S for technical support during the design of the various versions of AVID. Jacob Becker, Anette Gert Keilland, Thomas Bjørn Grønbech and Kristoffer Holm are gratefully acknowledged for their assistance in data the collection.

Funding information

The work was supported by the Danish National Research Foundation (DNRF93) and the Danish Agency for Science, Technology and Innovation (DANSCATT).

References

Alexander, L. & Klug, H. P. (1950). *J. Appl. Phys.* **21**, 137–142.
Bader, R. F. W. (2002). In *Encyclopedia of Computational Chemistry*. Chichester: Wiley.
Bergamaschi, A., Cervellino, A., Dinapoli, R., Gozzo, F., Henrich, B., Johnson, I., Kraft, P., Mozzanica, A., Schmitt, B. & Shi, X. (2010). *J. Synchrotron Rad.* **17**, 653–668.
Bindzus, N., Straasø, T., Wahlberg, N., Becker, J., Bjerg, L., Lock, N., Dippel, A.-C. & Iversen, B. B. (2014). *Acta Cryst.* A**70**, 39–48.
Birkedal, H., Madsen, D., Mathiesen, R. H., Knudsen, K., Weber, H.-P., Pattison, P. & Schwarzenbach, D. (2004). *Acta Cryst.* A**60**, 371–381.
Blessing, R. H. (1995). *Acta Cryst.* B**51**, 816–823.
Capelli, S. C., Bürgi, H.-B., Dittrich, B., Grabowsky, S. & Jayatilaka, D. (2014). *IUCrJ*, **1**, 361–379.
Coppens, P. (1997). *X-ray Charge Densities and Chemical Bonding*. IUCr/Oxford University Press.
Dippel, A.-C., Liermann, H.-P., Delitz, J. T., Walter, P., Schulte-Schrepping, H., Seeck, O. H. & Franz, H. (2015). *J. Synchrotron Rad.* **22**, 675–687.
Dovesi, R., Causa', M., Orlando, R., Roetti, C. & Saunders, V. R. (1990). *J. Chem. Phys.* **92**, 7402–7411.
Fischer, A., Tiana, D., Scherer, W., Batke, K., Eickerling, G., Svendsen, H., Bindzus, N. & Iversen, B. B. (2011). *J. Phys. Chem. A*, **115**, 13061–13071.
Fugel, M., Jayatilaka, D., Hupf, E., Overgaard, J., Hathwar, V. R., Macchi, P., Turner, M. J., Howard, J. A. K., Dolomanov, O. V., Puschmann, H., Iversen, B. B., Bürgi, H.-B. & Grabowsky, S. (2018). *IUCrJ*, **5**, 32–44.
Gatti, C. (2005). *Z. Kristallogr. Cryst. Mater.* **220**, 399–457.
Gatti, C., Saunders, V. R. & Roetti, C. (1994). *J. Chem. Phys.* **101**, 10686–10696.
Hirshfeld, F. L. (1977). *Theor. Chim. Acta*, **44**, 129–138.
Iversen, B. B., Larsen, F. K., Figgis, B. N., Reynolds, P. A. & Schultz, A. J. (1996). *Acta Cryst.* B**52**, 923–931.
Jayatilaka, D. & Dittrich, B. (2008). *Acta Cryst.* A**64**, 383–393.
Jørgensen, M. R. V., Hathwar, V. R., Bindzus, N., Wahlberg, N., Chen, Y.-S., Overgaard, J. & Iversen, B. B. (2014). *IUCrJ*, **1**, 267–280.
Kato, K., Hirose, R., Takemoto, M., Ha, S., Kim, J., Higuchi, M., Matsuda, R., Kitagawa, S., Takata, M., Garrett, R., Gentle, I., Nugent, K. & Wilkins, S. (2010). *AIP Conf. Proc.* pp. 875–878.
Kato, K. & Tanaka, H. (2016). *Adv. Phys. X*, **1**, 55–80.
Koritsanszky, T. S. & Coppens, P. (2001). *Chem. Rev.* **101**, 1583–1627.
Le Bail, A., Duroy, H. & Fourquet, J. L. (1988). *Mater. Res. Bull.* **23**, 447–452.
Madsen, A. Ø., Civalleri, B., Ferrabone, M., Pascale, F. & Erba, A. (2013). *Acta Cryst.* A**69**, 309–321.
Madsen, A. Ø., Sørensen, H. O., Flensburg, C., Stewart, R. F. & Larsen, S. (2004). *Acta Cryst.* A**60**, 550–561.
Meindl, K. & Henn, J. (2008). *Acta Cryst.* A**64**, 404–418.
Morgenroth, W., Overgaard, J., Clausen, H. F., Svendsen, H., Jørgensen, M. R. V., Larsen, F. K. & Iversen, B. B. (2008). *J. Appl. Cryst.* **41**, 846–853.
Nishibori, E., Sunaoshi, E., Yoshida, A., Aoyagi, S., Kato, K., Takata, M. & Sakata, M. (2007). *Acta Cryst.* A**63**, 43–52.
Petříček, V., Dušek, M. & Palatinus, L. (2014). *Z. Kristallogr.* **229**, 345–352.
Pichon-Pesme, V., Lecomte, C. & Lachekar, H. (1995). *J. Phys. Chem.* **99**, 6242–6250.
Seeck, O. H., Deiter, C., Pflaum, K., Bertam, F., Beerlink, A., Franz, H., Horbach, J., Schulte-Schrepping, H., Murphy, B. M., Greve, M. & Magnussen, O. (2012). *J. Synchrotron Rad.* **19**, 30–38.
Spackman, M. A. & Byrom, P. G. (1997). *Acta Cryst.* B**53**, 553–564.
Spackman, M. A., Byrom, P. G., Alfredsson, M. & Hermansson, K. (1999). *Acta Cryst.* A**55**, 30–47.
Stephens, P. W. (1999). *J. Appl. Cryst.* **32**, 281–289.
Straasø, T., Becker, J., Iversen, B. B. & Als-Nielsen, J. (2013). *J. Synchrotron Rad.* **20**, 98–104.
Svendsen, H., Overgaard, J., Busselez, R., Arnaud, B., Rabiller, P., Kurita, A., Nishibori, E., Sakata, M., Takata, M. & Iversen, B. B. (2010). *Acta Cryst.* A**66**, 458–469.
Swaminathan, S., Craven, B. M. & McMullan, R. K. (1984). *Acta Cryst.* B**40**, 300–306.
Tolborg, K., Jørgensen, M. R. V., Christensen, S., Kasai, H., Becker, J., Walter, P., Dippel, A.-C., Als-Nielsen, J. & Iversen, B. B. (2017). *Acta Cryst.* B**73**, 521–530.
Volkov, A., Messerschmidt, M. & Coppens, P. (2007). *Acta Cryst.* D**63**, 160–170.
Vries, R. Y. de, Feil, D. & Tsirelson, V. G. (2000). *Acta Cryst.* B**56**, 118–123.

Wahlberg, N., Bindzus, N., Bjerg, L., Becker, J., Christensen, S., Dippel, A.-C., Joergensen, M. R. & Iversen, B. B. (2015). *J. Phys. Chem.* **119**, 6164–6173.
Wahlberg, N., Bindzus, N., Bjerg, L., Becker, J., Dippel, A.-C. & Iversen, B. B. (2016). *Acta Cryst.* A**72**, 28–35.
Wall, M. E. (2016). *IUCrJ*, **3**, 237–246.
Weidenthaler, C. (2011). *Nanoscale.* **3**, 792–810.
Woińska, M., Grabowsky, S., Dominiak, P. M., Woźniak, K. & Jayatilaka, D. (2016). *Sci. Adv.* **2**, e1600192.
Woińska, M., Jayatilaka, D., Spackman, M. A., Edwards, A. J., Dominiak, P. M., Woźniak, K., Nishibori, E., Sugimoto, K. & Grabowsky, S. (2014). *Acta Cryst.* A**70**, 483–498.
Zavodnik, V., Stash, A., Tsirelson, V., de Vries, R. & Feil, D. (1999). *Acta Cryst.* B**55**, 45–54.